Chapter 3
Time Domain Component Based TPA on the Round Robin Structure

Steven Carter

Abstract Component based transfer path analysis (TPA) is a popular technique because it can be used to translate vibration environments from one system to another. Work has been presented at recent IMACs where the method was used in the frequency domain to translate random vibration environments between different versions of the round robin structure for the substructuring technical division of SEM. This previous work demonstrated the use of different regularization schemes to mitigate overfitting errors in the force estimation step, which dramatically improved the accuracy of the environment translation. This paper builds on the previous work, but with a focus on a transient vibration environment that combines sine, random, and shock excitation, which required a time domain force estimation scheme. It will demonstrate the use of TPA techniques in the time domain and discuss extra challenges that weren't experienced in the frequency domain with the random vibration environment.

Keywords TPA · Substructuring round robin · Force estimation · Inverse methods · Equivalent source

Introduction

Component based transfer path analysis (CB-TPA) [1–6] has become a popular technique because it can be used to translate vibration environments between versions of a system. The CB-TPA framework leverages the source-path-receiver description of the system, which can be summarized as:

- Source – The component(s) in a system that are subjected to a motive force. Examples of source components include the engine/motor in a car or the rocket motor on a missile.
- Receiver – The component(s) in a system that passively respond to the vibrations from the source component(s). Examples of receiver components include the body in a car or the payload in a missile.
- Path – The connection that transfers vibration energy between the source and receiver components in a system. Example paths include engine mounts or bolted joints.

In CB-TPA, so-called equivalent sources are estimated on the source component of a system and are used to predict the vibration responses on the receiver components. These equivalent sources only depend on the dynamics of the source component. Consequently, they can be used to predict the vibration response of the receiver component in a modified version of a system, provided that the source component remains the same. A common example of CB-TPA is to describe the powertrain forces in a car with an equivalent source. These equivalent sources are then be applied to source-path-receiver models of different vehicle configurations to predict how the sound and vibration changes with the vehicle configuration changes.

Different methods exist to estimate the equivalent sources, but the matrix inversion method is likely the most common. This method is shown in shown in (1).

$$\{F\} = [H]^{+}\{X\} \tag{1}$$

Steven Carter
Sandia National Laboratories, P.O. Box 5800 – MS0557, Albuquerque, NM, 87185
e-mail: spcarte@sandia.gov

Kristin B. Zimmerman, PhD (eds.), *Dynamic Substructuring & Transfer Path Analysis, 2026, Vol. 4*, Conference Proceedings of the Society for Experimental Mechanics Series, https://doi.org/10.1007/978-8-743-81443-6_3

In this equation, $\{F\}$ is a vector of estimated equivalent sources (referred to as forces from now on), $[H]$ is the frequency response function (FRF) matrix description of the assembled source-path-receiver system, $\{X\}$ is a vector of measured vibration responses on the receiver component(s) of the system, and $[\cdots]^+$ indicates the pseudo-inverse of the given quantity. Note that all these quantities have a frequency dependency, but this notation was left out for brevity.

The physics for the CB-TPA framework have thoroughly proven the validity of the forces that are estimated with matrix inversion (in the absence of measurement errors). However, it has been shown that errors in the responses and FRFs can cause erroneous overfit forces [7–9], which are not valid for predicting the vibration responses on modified systems. Thankfully, there has been significant research into improving the robustness of the matrix inversion process [10–18] to these errors.

Previous work [17] demonstrated the use of some of these improved inverse methods for a random vibration environment that was applied to the round robin structure (RRS) for the substructuring technical division of the Society for Experimental Mechanics (SEM) [19, 20]. This paper builds on the previous work and applies the CB-TPA framework with advanced inverse methods to the RRS for a transient environment. It will discuss the following:

- The experimental set-up to generate "truth" vibration responses for two versions of the RRS
- The problem set-up for the force estimation and response prediction
- The force estimation and response prediction results, compared to the truth vibration responses
- The challenges that were experienced in the CB-TPA process for transient environments

Experimental Set-up

The truth data that was used in this work was gathered in a multiple-input / multiple-output (MIMO) vibration test using the Rattlesnake vibration controller [21]. The goal of the MIMO test was to provide the same motive forces to the frame of the RRS when the system was in two different configurations. For this work, the frame was considered the source component, and the wing was considered the receiver component. The two configurations were the thick (0.25" thick) and thin (0.125" thick) straight wing. The wing was bolted to the frame with four bolts, as shown in Figure 1, which were torqued to 68 in*lbs. Note that washers were placed between the frame and wing at each bolt location to linearize the system response, although they cannot be seen in the pictures.

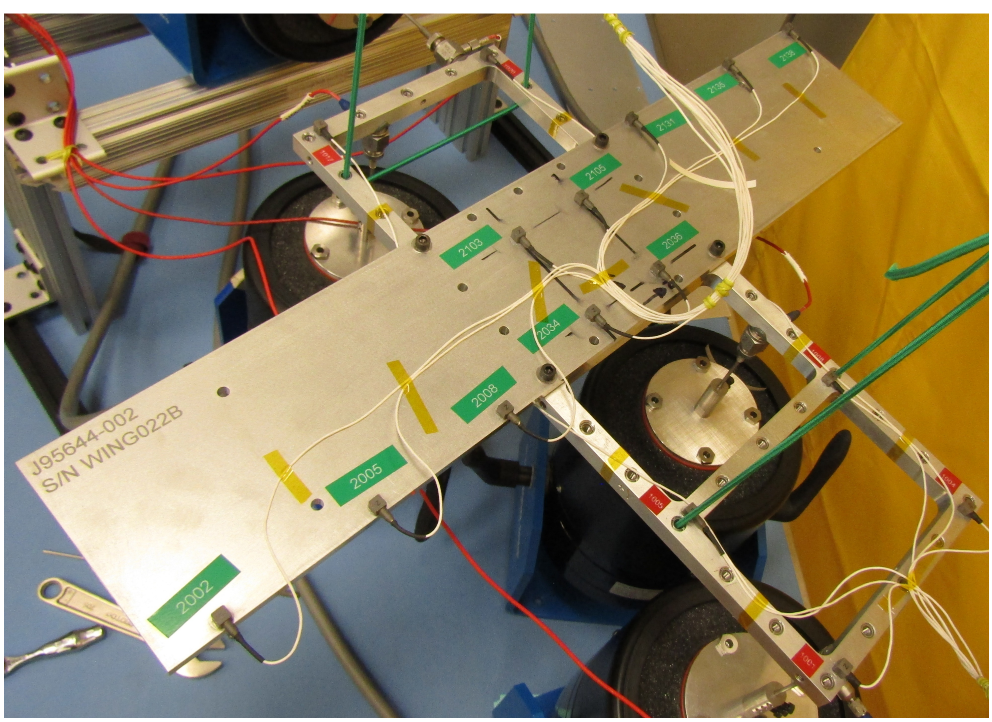

Fig. 1 Accelerometer and bolted joint locations for the MIMO vibration test

The MIMO vibration test set-up is shown in Figure 2. The four shakers and corresponding load cell locations that were used as the control degrees of freedom (DOFs) for the test can also be seen in this image. The bungee cords (the green lines) that were used to support the system in an approximated free-free boundary condition are shown in this image as well. There were sixteen triaxial accelerometer locations in the test, which are the grey cubes with white cables that are near the green and red labels, as shown in Figure 1. Note that the response locations on the wing roughly match the previous work [8, 17].

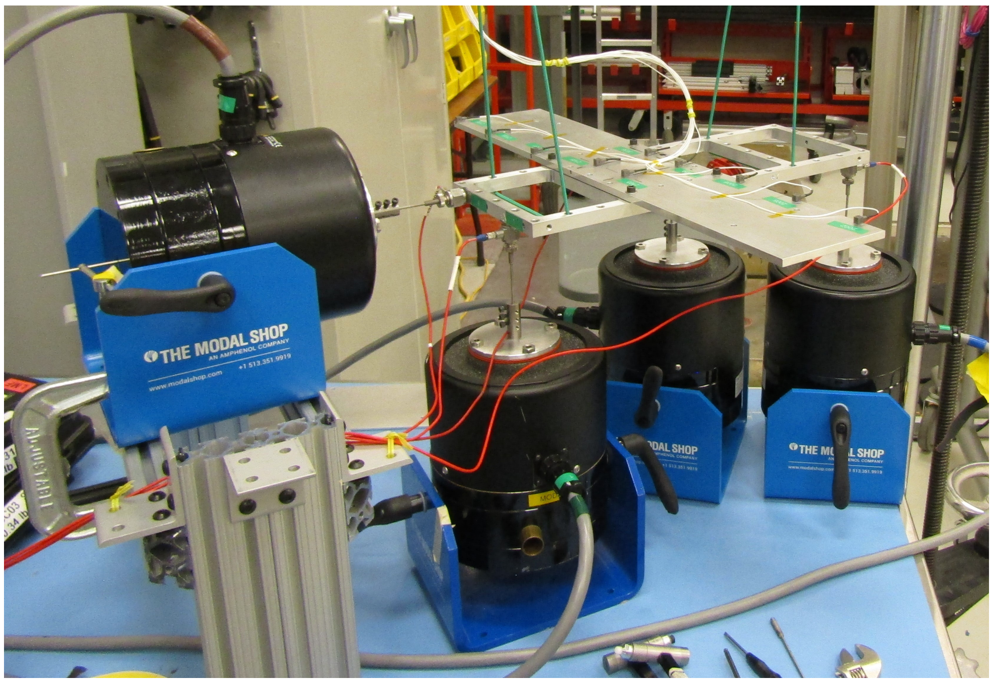

Fig. 2 MIMO vibration test set-up for gathering truth data

The transient vibration environment for this work had sine, random, and shock excitation superimposed on each other. An example force time trace for a single control DOF is shown in Figure 3 and an example spectrogram is shown in Figure 4. The process for generating the transient environment was:

1. A time-varying drive voltage signal with superimposed random and chirp content was created for each shaker. These drive signals were created in a random fashion, where the modulation shape, chirp start-stop times and frequencies, and signal amplitudes were selected with random number generators. Also note that the signal duration was selected to be computationally demanding for the force estimation algorithms.
2. The drive signals were played through the shakers while the frame and wing were impacted with a hammer at random time intervals and locations to add shock content while responses were being measured with the accelerometers.
3. The measured responses from step two were filtered with a passband of 20-4,000 Hz.
4. A response-controlled MIMO vibration test was performed on the thick wing RRS configuration, using the filtered vibration responses from step three. Note that steps 1-4 were repeated if a reasonably accurate MIMO test could not be performed within the capabilities of the test set-up (which was generally limited by the shock amplitudes). This test provided the truth response data for the thick wing RRS configuration.
5. The measured forces from step four were bandpass filtered with a passband of 20-4,000 Hz. The filtered forces were the specification for the force-controlled MIMO test that was used to develop the truth data for thin wing RRS configuration.

The vibration control for the force-controlled MIMO test on the thin wing RRS was performed as a MIMO time waveform replication (TWR) test. The control was done "offline" using the constant overlap and add (COLA) algorithm that is in the SDynPy Python package [22, 23]. An abridged description of this control algorithm is:

1. System identification (ID) FRFs are measured between the shaker drives and control DOFs via a low-level random vibration test.

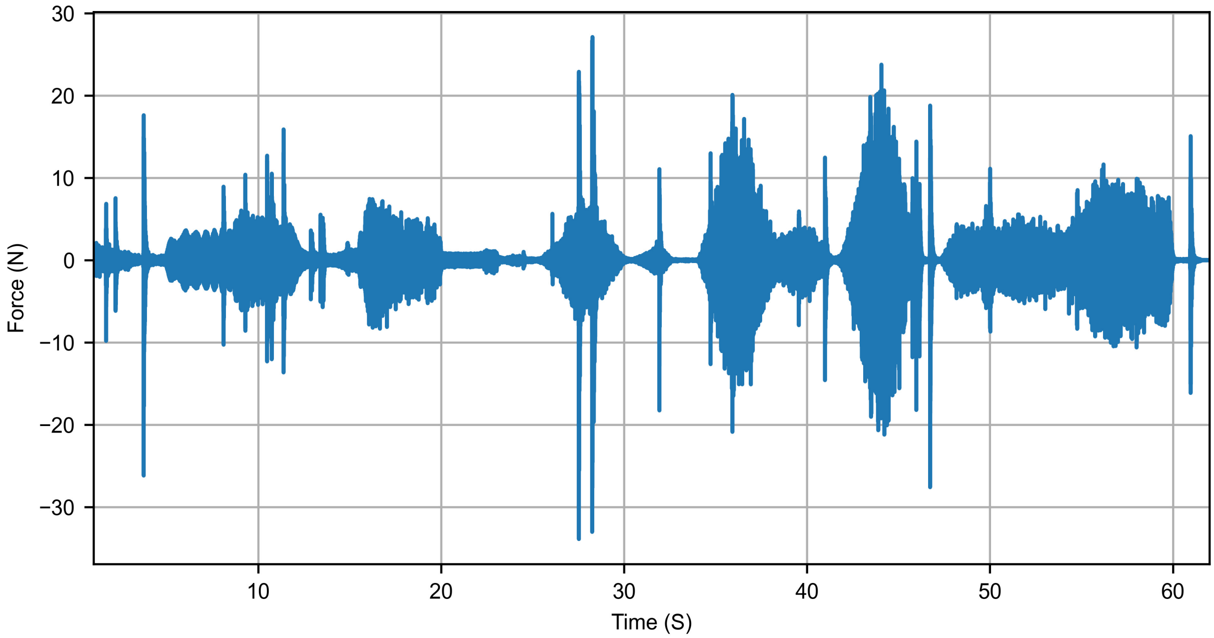

Fig. 3 Sample force time trace for the transient environment

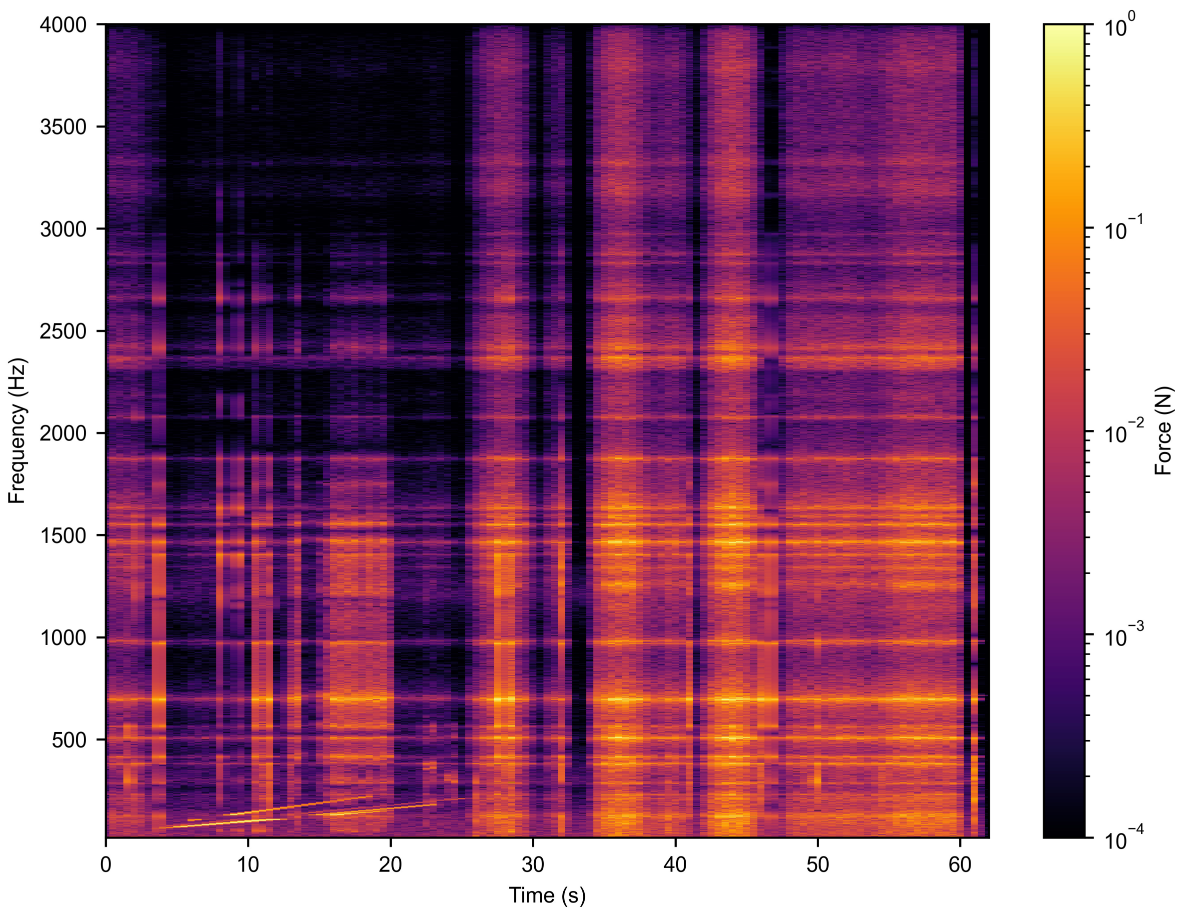

Fig. 4 Sample force spectrogram for the transient environment

2. The full-length specification time trace is zero padded to avoid any spoilage from the windowing in the COLA algorithm.

3. The response time trace (from step two) is split into overlapped and windowed segments. In this case, a hann window was used with 50% overlap.

4. The specification segments (from step three) are zero padded to avoid any convolution wraparound errors [24, 25].

5. The windowed, segmented, and zero padded specification (from step four) is converted to the frequency domain with a discrete Fourier transform (DFT).

6. The system ID FRFs are interpolated to match the number of samples in the frequency domain specification (from step five).

7. The frequency domain specification (from step five) and interpolated FRFs (from step six) are used to estimate the drive voltages via FRF matrix inversion. Tikhonov regularization [26] (with a regularization parameter of one) was used in the control problem to reduce the required drive voltage and sensitivity to noise while maintaining reasonable accuracy.

8. The frequency domain drive voltages (for each time segment) are converted to the time domain using an inverse DFT.

9. The segmented time domain drive voltages (from step eight) are recompiled into a single time trace for the whole time.

10. The full-length drive voltages (from step nine) are played through the shaker system to achieve the desired response.

The Tikhonov regularization formulation for the inverse problem (from step seven in the control algorithm) is shown in (2). This inverse problem is solved with the singular components of the FRF matrix that are computed with the singular value decomposition [27], as shown in (3).

$$[H]^{+} = [V] \frac{[S]}{[S]^{2} + \lambda} [U]^{*} \tag{2}$$

$$[H] = [U] [S] [V]^{*} \tag{3}$$

In these equations, $[V]$ is a square matrix of the right singular vectors of the FRF matrix, $[S]$ is a diagonal matrix of the singular values of the FRF matrix, $[U]$ is a rectangular matrix of the left singular vectors of the FRF matrix, λ is the (tunable) regularization parameter, and $[\cdots]^{*}$ indicates the conjugate-transpose of the given matrix.

The accuracy of the force-controlled MIMO test on the thin wing RRS configuration was rated with in depth subjective comparisons between the test and specification time traces. Unfortunately, it is difficult to show the comparisons for this highly transient environment without interactive plotting. Consequently, two metrics are used to demonstrate control accuracy:

1. Running Root Mean Square (RMS) Error – This metric splits the control and specification time traces into one second frames with 50% overlap. The RMS level is then computed for the test and specification, which are then compared and converted to decibels (dB).

2. Running Time Response Assurance Criterion (TRAC) – This metric splits the control and specification time traces into one second frames with 50% overlap. A TRAC comparison is then done between the test and specification time traces to evaluate test accuracy.

The running RMS error and TRAC comparisons for the force-controlled MIMO test on the thin wing RRS configuration are shown in Figure 5 and Figure 6, respectively. These metrics show that the test and specification time traces generally had a similar amplitude and shape for both RRS configurations, which matches the subjective comparisons. There is a moderate discrepancy in the test-specification comparisons at $\sim$8 seconds, but this was deemed acceptable, given the purpose of the test.

Based on the test-specification comparisons, it was determined that both RRS configurations were subjected to the same motive forces. and the response data was deemed to be suitable for evaluating CB-TPA methods in transient environments. However, it should be noted that there may have been some discrepancies that were caused by unmeasured off-axis loads. It is assumed that this off-axis loading (if any existed) was small in comparison to the controlled forces. Further, it is assumed that any discrepancies in the motive forces from this testing would be less than what is typical in an actual field test.

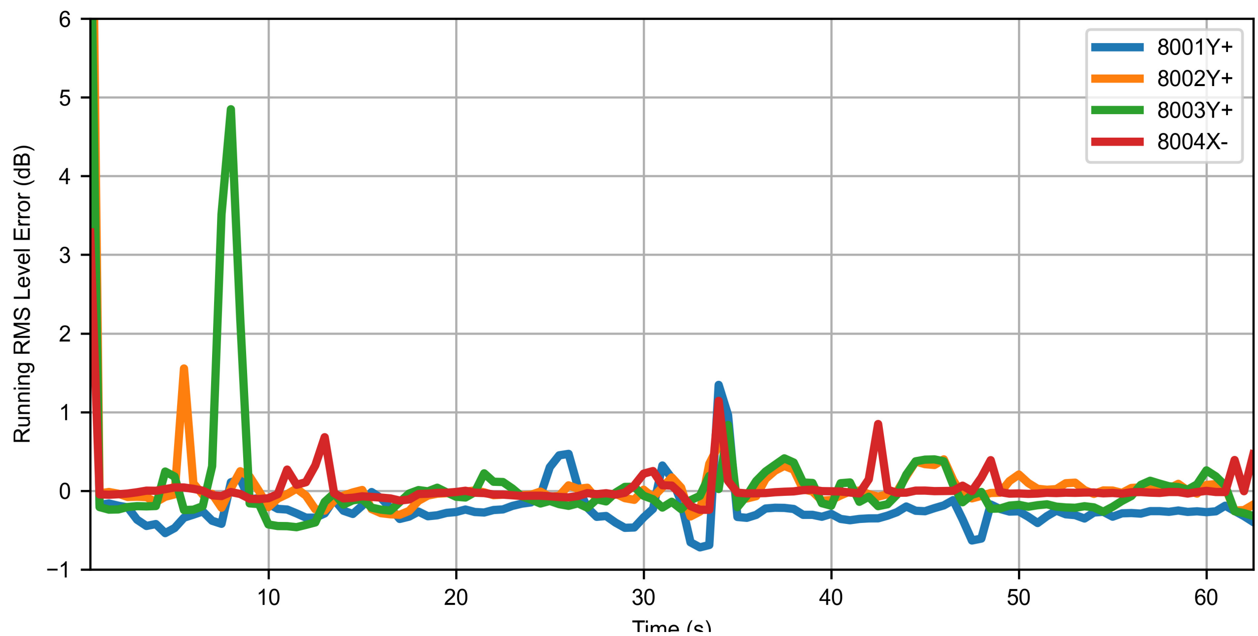

Fig. 5 Running test-spec RMS error for the force-controlled MIMO test on the thin wing RRS configuration

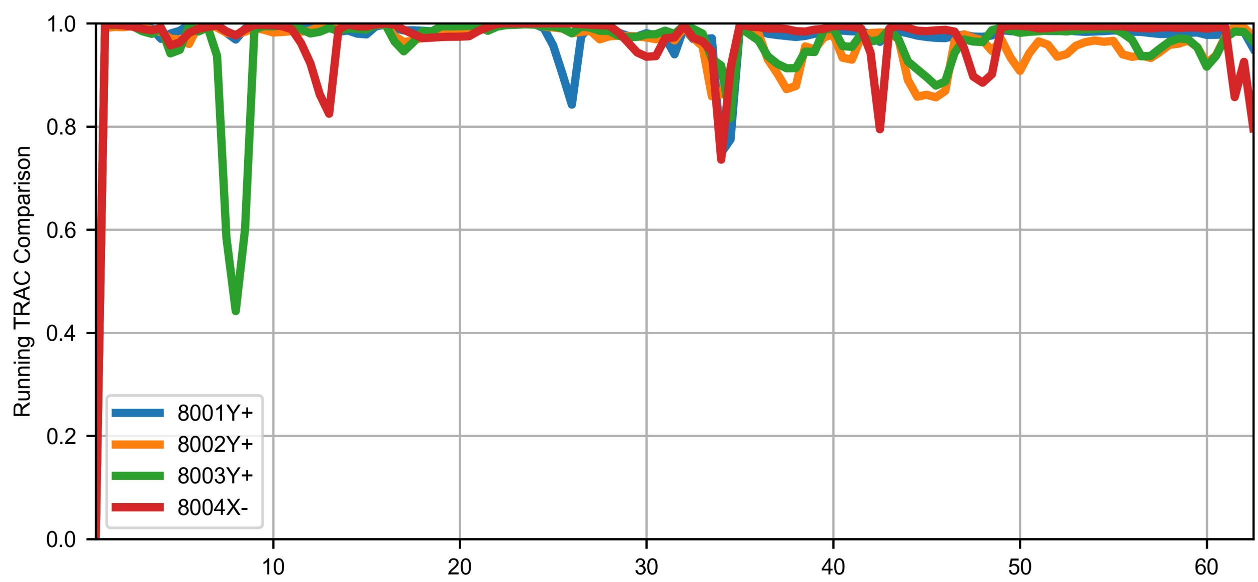

Fig. 6 Running test-spec TRAC comparison for the force-controlled MIMO test on the thin wing RRS configuration

Force Estimation and Response Prediction Set-up

Both the force estimation and response prediction were performed with a so-called hybrid framework to mimic a typical aerospace scenario, where sufficient FRF data (for the TPA process) is unavailable for a flight test asset. As such, the FRFs were generated from calibrated finite element (FE) models for both versions of the system (with a modal damping ratio of 2%), that had been developed in the previous work [8]. The response data came from the accelerometers that were mounted to the wing in the previously described tests. Note that the FE model was created and calibrated for the previous TPA work [8, 17]. This previous work used an RRS specimen that is nominally, but not exactly, the same as the RRS specimen that was tested for this work. It was assumed that the different RRS specimens will have the same modal properties, but this was not confirmed.

It should be noted that the FRFs from the FE model have significant “apparent non-causalities”, which have been found to cause problems in MIMO TWR problems [28]. An example of the apparent non-causality is shown in Figure 7, where there is a sudden rise at the end of a sample impulse response function (IRF) that was computed via the inverse DFT of one of the FRFs. This issue was mitigated by enforcing causality in the FRFs using the enforce_causality method (with default settings) in SDynPy, which implements the method that is detailed in [29]. Six DOF (translation and rotation) forces were estimated at the bolted joints between the frame and wing (24 total force DOFs). This problem form matches the previous work, which was able to predict random vibration responses with good accuracy.

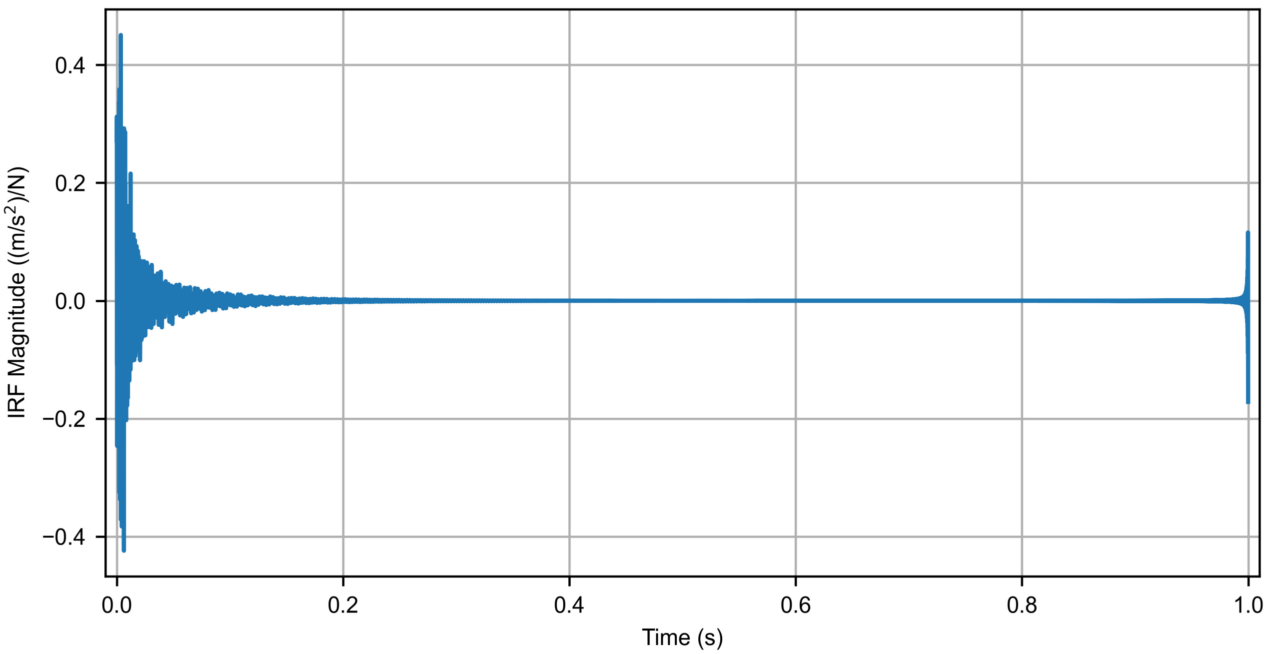

Fig. 7 Sample IRF showing non-causal behavior

The ForceFinder Python package [30] was used to estimate the forces. The process was very similar to the MIMO TWR process that was described in Section Error! Reference source not found., with some minor modifications in the COLA algorithm for computational efficiency. Unless otherwise noted, pre-implemented ForceFinder methods were used with the default settings to estimate the forces. The results for two different inverse methods will be shown in this work:

1. Standard pseudo-inverse (referred to as pinv). This is the manual_inverse method in ForceFinder with the inverse_method kwarg set to standard.
2. Tikhonov regularization with automatic parameter selection via the L-curve (referred to as auto-Tikhonov). This is the auto_tikhonov_by_l_curve method in ForceFinder. Note that this algorithm generates an L-curve and selects a regularization parameter for every frequency line in every time segment. Some optional kwargs were different than the defaults. The optional inputs were:
   a. The l_curve_type kwarg that was set to standard
   b. The optimality_condition kwarg that was set to distance
   c. The number_regularization_values kwarg that was set to 30.

Lastly, it should be noted that the forces were estimated on the thick wing RRS configuration. The estimated forces were then applied to the thin wing RRS configuration to predict the vibration response and compare it to the measured data.

Results

This section describes the results for the force estimation and response prediction on both RRS configurations. Like the force-controlled MIMO test, in depth comparisons (including listening to audio files of the responses) were done between the test and predicted response time traces. However, those comparisons cannot be shown in this paper. The time trace comparisons are further complicated by the relatively large number of response DOFs that are in the predictions. As such, two summary metrics are being used to show the accuracy of the response predictions compared to the test response:

- Global RMS error [31] – This is a summary metric that is defined in MIL-STD 810 for MIMO TWR tests. It is a DOF-averaged version of running RMS error where the DOFs are weighted according to their maximum response amplitude in comparison to the other DOFs. This metric is useful for understanding if the forces are predicting responses with roughly the same levels as the test data.
- DOF-averaged TRAC – This is a summary metric that averages the running TRAC metric for every response DOF. This metric is useful for understanding if the forces are predicting the correct response waveform.

The first comparisons show the force estimation and response reconstruction results (i.e., recomputing the responses from the estimated forces) on the thick wing RRS configuration. These comparisons are used to validate that the forces reasonably capture the dynamics of the system and build confidence that they can be used to predict responses on other RRS configurations. The DOF-averaged running RMS level for the forces from the different inverse methods is shown in Figure 8. As expected, the force levels are significantly lower for the auto-Tikhonov method, compared to the pinv method. The global RMS error is shown for the reconstructed responses (from the estimated forces) on the thick wing RRS in Figure 9. This figure shows that both the pinv and auto-Tikhonov inverse methods recreate the response amplitudes with good accuracy. However, the regularization seems to cause bias error, where the reconstructed response levels are slightly lower than the test.

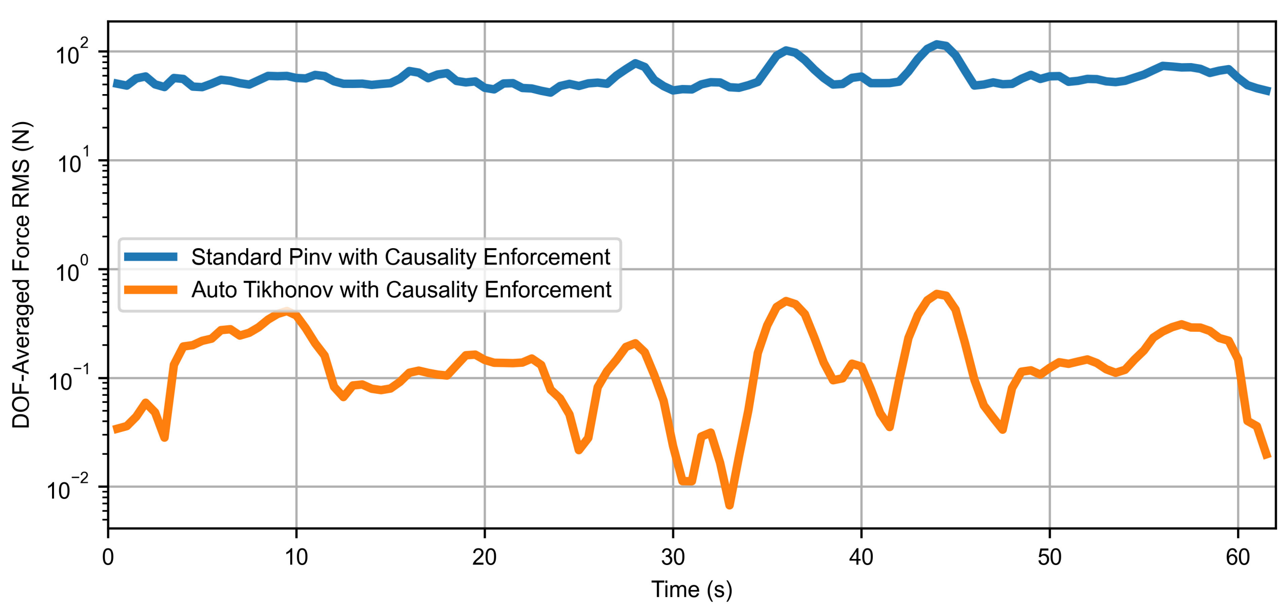

Fig. 8 DOF-averaged running RMS level for the forces from both inverse methods

The DOF-averaged TRAC is shown in Figure 10, which shows that the waveform shapes for the reconstructed responses match the test reasonably well for both inverse methods. Like the global RMS error, the DOF-averaged TRAC shows more error for the auto-Tikhonov method compared to the pinv method. However, the errors in the reconstructed responses for both inverse methods on the thick wing RRS were deemed acceptable.

Lastly, a sample time trace comparison between the reconstructed and test responses for the thick wing RRS is shown in Figure 11 for a single response DOF from the auto-Tikhonov method. Note that the reconstructed response is transparent in this figure, which means that the brown portions are where the reconstructed and test responses overlay. This figure shows that the reconstructed responses have the same general character, shape, and amplitude as the test response.

The global RMS error for the predicted responses on the thin wing RRS configuration (from forces that were estimated with thick wing data) is shown in Figure 12 for both inverse methods. This figure shows that the forces from the pinv method dramatically overpredict the response amplitude on the thin wing RRS, which indicates that the forces were overfit with this

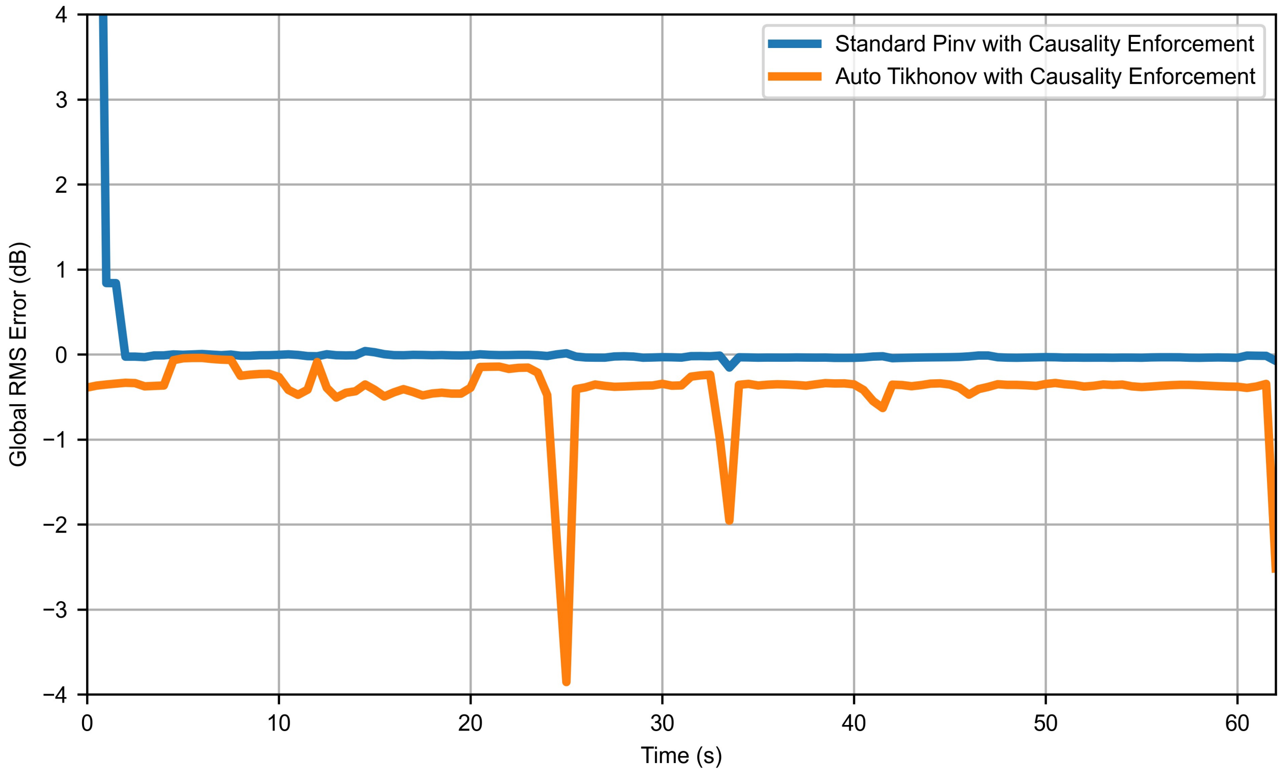

Fig. 9 Global RMS error of the reconstructed responses on the thick wing RRS of both inverse methods

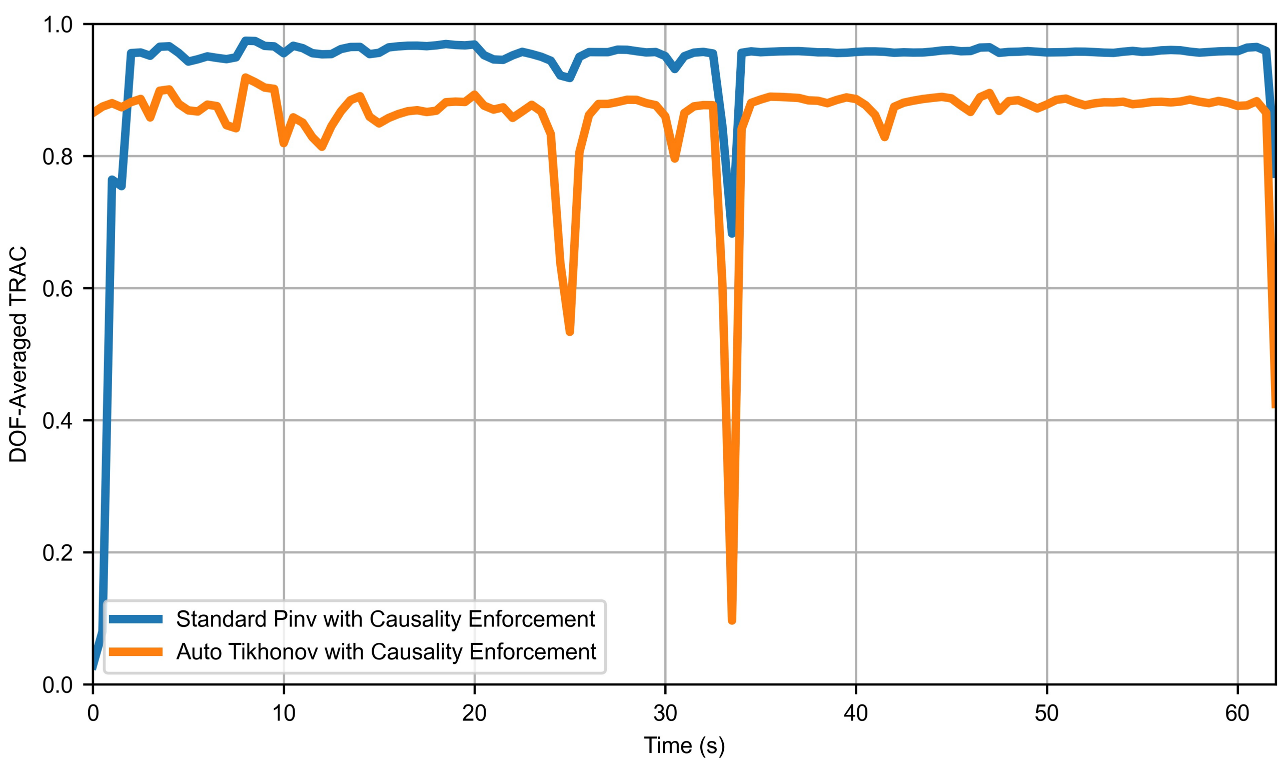

Fig. 10 DOF-averaged running TRAC of the reconstructed responses on the thick wing RRS of both inverse methods

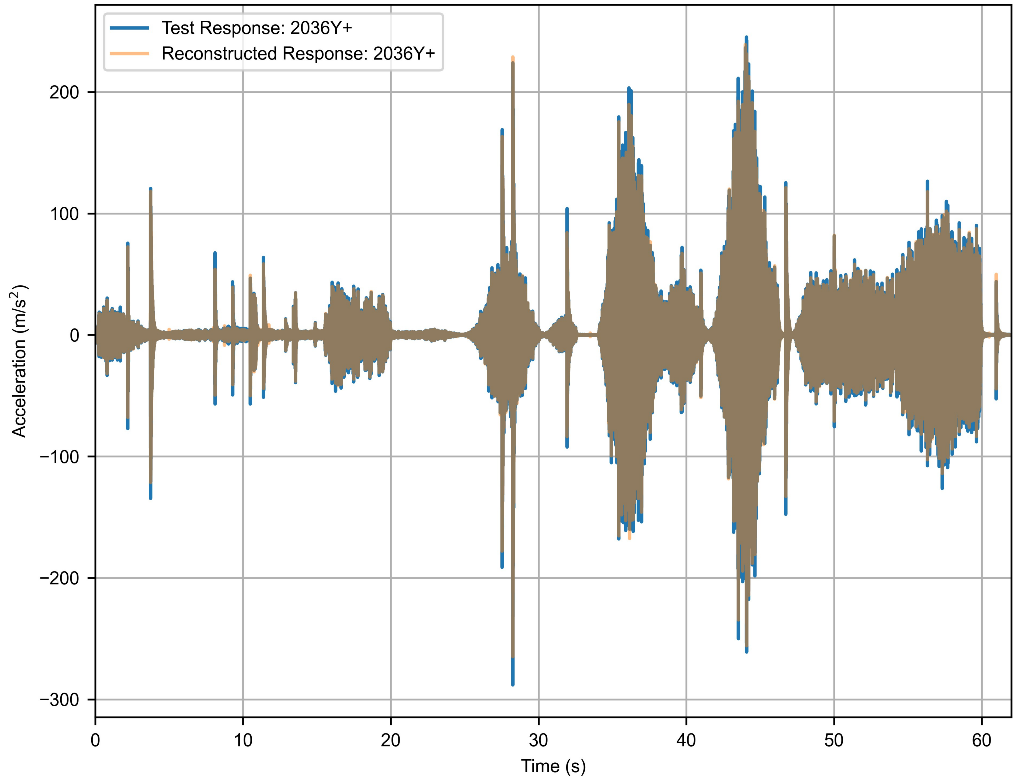

Fig. 11 Sample time trace comparison between the reconstructed and test response on the thick wing RRS for the auto-Tikhonov method, the trace for the reconstructed response is transparent, meaning that the brown parts are where the reconstructed and test response overlay

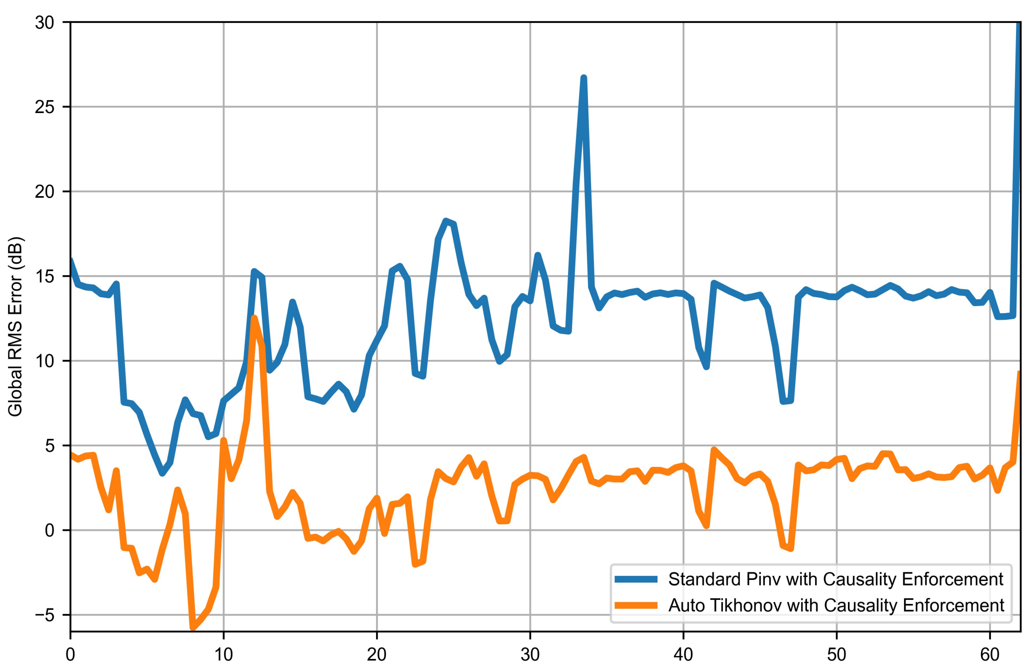

Fig. 12 Global RMS error of the predicted responses on the thin wing RRS for both inverse methods

method. The predicted response amplitudes from the auto-Tikhonov forces are much more accurate, but still tend to result in an overprediction.

The DOF-averaged TRAC for the predicted response on the thin wing RRS is shown in Figure 13, which shows that forces from both inverse methods poorly predict the response waveform. Note that this error is somewhat expected, since modelling errors will have a significant impact on the phase and resulting waveform shape, which TRAC is very sensitive to. A sample time trace comparison between the predicted and test responses is shown in Figure 14 for the pinv method and Figure 15 for the auto-Tikhonov method.

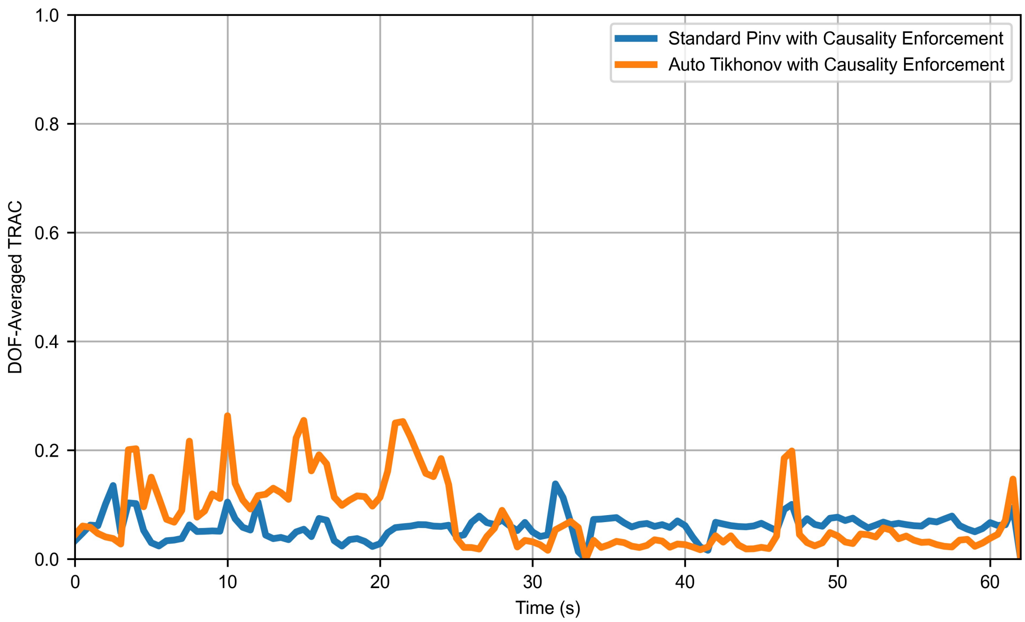

Fig. 13 DOF-averaged running TRAC of the predicted responses on the thin wing RRS for both inverse methods

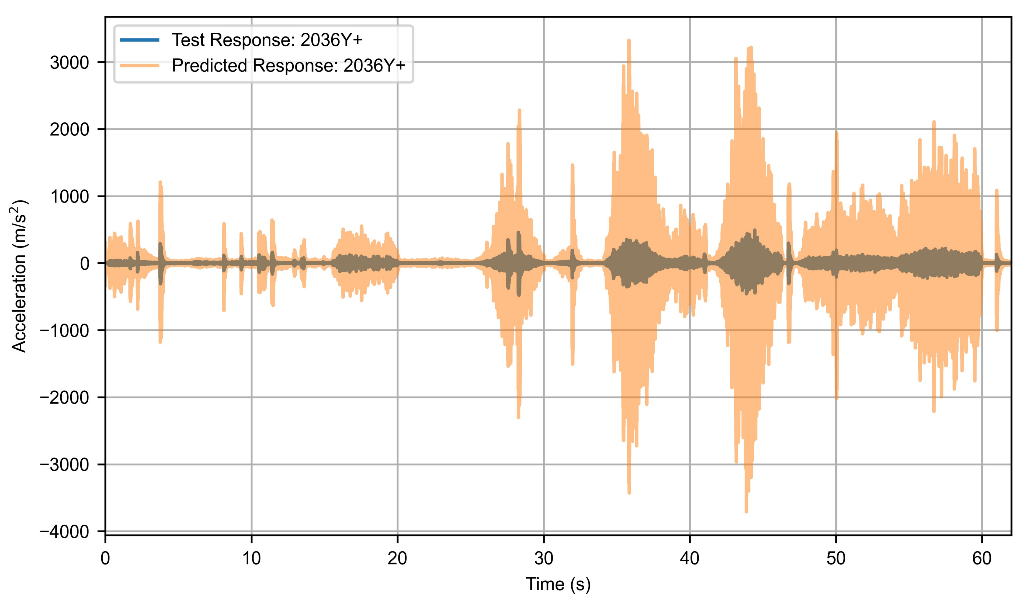

Fig. 14 Sample time trace comparison between the predicted and test response on the thin wing RRS for the pinv method, the trace for the predicted response is transparent, meaning that the brown parts are where the reconstructed and test response overlay

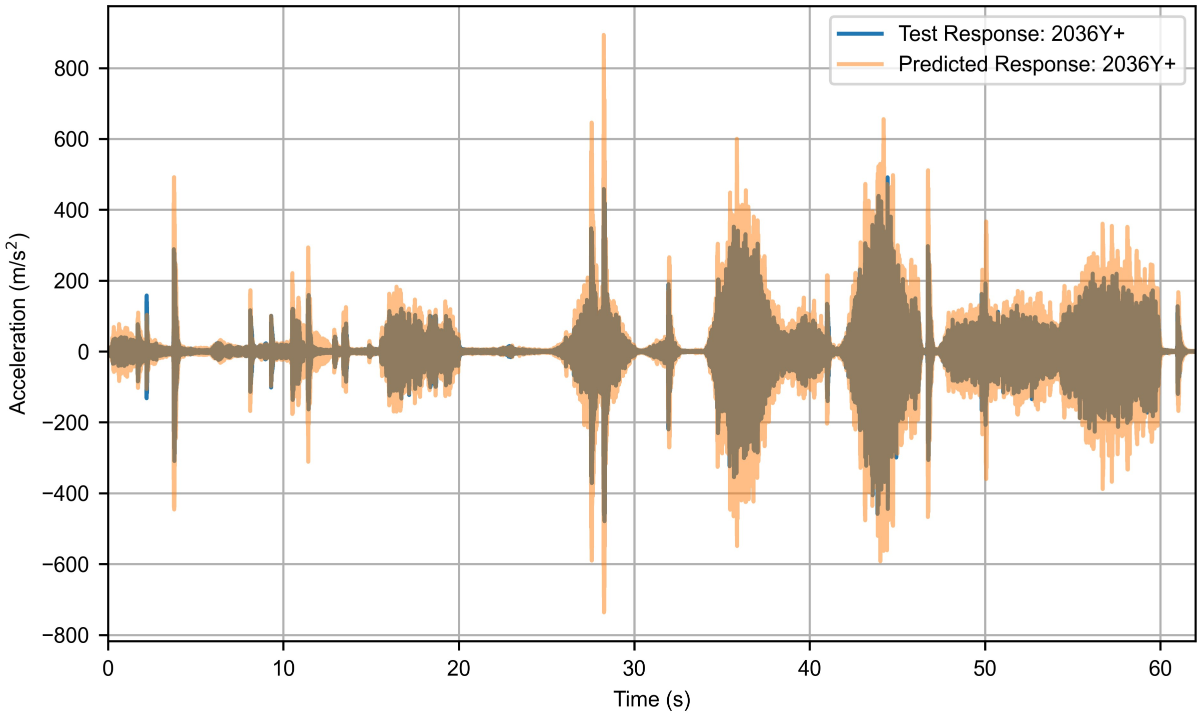

Fig. 15 Sample time trace comparison between the predicted and test response on the thin wing RRS for the auto-Tikhonov method, the trace for the predicted response is transparent, meaning that the brown parts are where the reconstructed and test response overlay

The time trace comparisons show that the forces from both inverse methods generally predict the correct shape of the response time trace, although the pinv method results in excessive response amplitudes. Further, the character and shape of the predicted responses better match the test responses when the auto-Tikhonov forces are used, especially around the impulses. The auto-Tikhonov predicted responses tend to show distinct impulses whereas the impulses for the pinv predicted responses tend to blend in with the surrounding content, especially for the impulses in the 25-30 second time region.

Discussion: regularization Settings

The results in this work confirmed that the L-curve Tikhonov regularization algorithm could be used to significantly improve the predictive quality of pseudo-forces in a transient environment, compared to a standard pseudo-inverse. This improvement was primarily demonstrated in through the global RMS error and direct time trace comparisons. Additional in-depth comparisons of the time traces, running RMS error, error spectrograms, and subjective listening studies (where the vibration responses were converted to audio files) also confirmed this finding. However, it is difficult to show the in-depth comparisons in this format.

The listening study highlighted that the predicted responses (from the forces for both inverse methods) tended to have high frequency “ringing” that was not present in the test response. This ringing was much worse for the forces from pinv method. The listening study also indicated that the predicted responses from the auto-Tikhonov forces captured the “character” of the test responses better than the pinv forces.

Although it was not discussed elsewhere in this work, it was found that some inverse settings (changes in regularization, frequency dependent weightings, etc.) may cause spurious peaks in the forces, and hence the predicted responses. A sample reconstructed response with the spurious peaks is shown in Figure 16. This curve was generated by simply changing how the L-curve algorithm selected the regularization parameter when estimating the forces, with no other changes to the problem set-up. The cause of the spurious peaks is unknown, but it is hypothesized that the regularization is acting as a non-causal filter, like what would happen if causality was not enforced on the FRFs. Further work is needed to fully understand the cause for these spurious peaks.

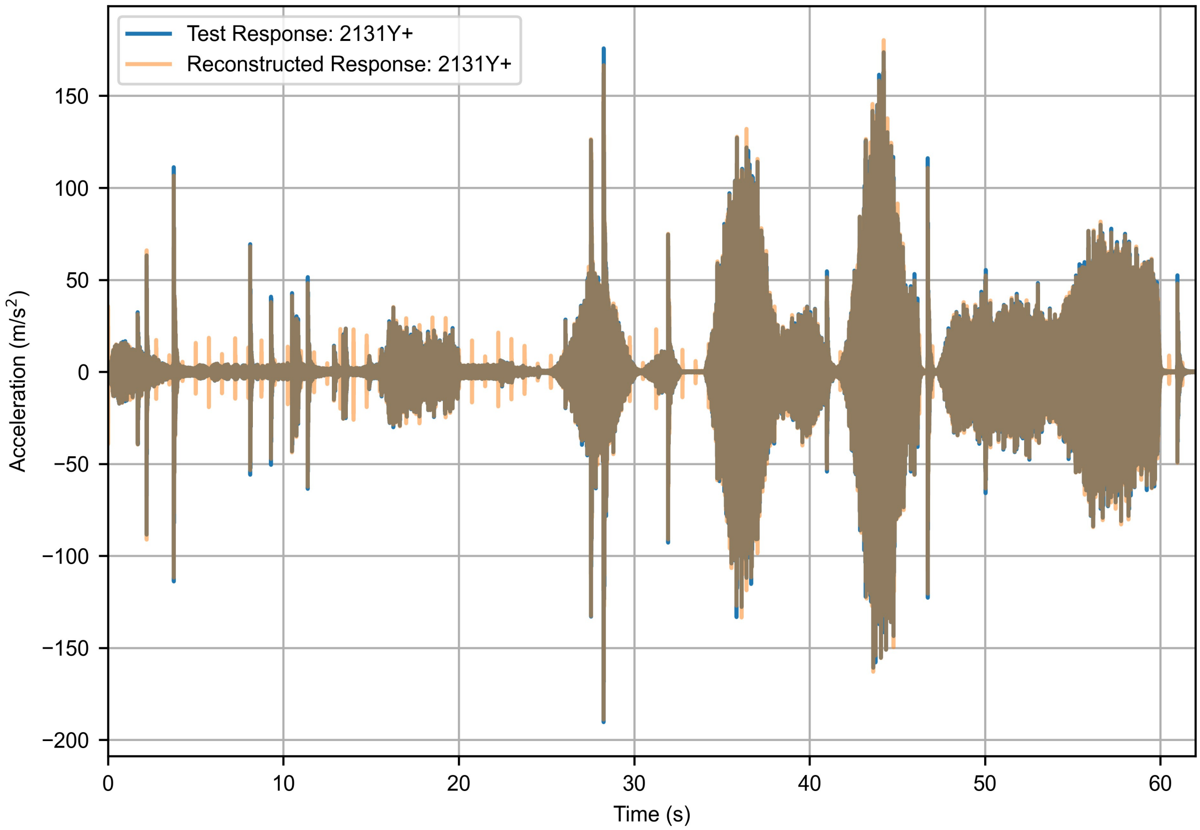

Fig. 16 Sample time trace comparison between the reconstructed and test response on the thick wing RRS with different inverse setting that show apparent non-causality, the trace for the reconstructed response is transparent, meaning that the brown parts are where the reconstructed and test response overlay

Discussion: Challenges in Evaluating Response Prediction Accuracy

It was extremely difficult to evaluate the accuracy of the predicted responses compared to the test responses. Naively, initial attempts were made to directly compare the response waveforms (via a visual inspection and correlation metrics). However, it was found that several seemingly insignificant errors in the prediction could cause dramatic issues in the comparisons. Examples of these errors include:

- Minor phase errors or frequency shifts that are due to generally acceptable modeling errors (e.g., +/-5% natural frequency error) could cause dramatic differences in how sine waves are superimposed on each other
- Minor errors in time axis alignment causing dramatic differences in the waveform comparisons
- Spurious tones that make the waveform look completely wrong, when the error is only in a small frequency band

Spectrograms were also used to evaluate the accuracy of the response predictions. This was done by computing the spectrum error (in dB) for a short-time Fourier transform of the predicted and test responses. These plots provided useful information since it was possible to visualize the frequencies and moments in time where there were errors. However, it was difficult to interpret the spectrograms to determine if the identified errors were significant to the overall response. This is because the error calculation eliminates any sense of the response amplitude. For example, the error spectrogram could show high error, but that error might occur at a time or frequency that is has a low response amplitude, meaning that the error is insignificant to the overall response. The error calculation could be normalized to response amplitude, but it is unclear if this could be justified in general use.

It was found that many metrics (include waveform and spectrogram comparisons) provided an overwhelming amount of information that was difficult to track. This overwhelming amount of information was compounded by the high number of channels for the response predictions. As such, some metrics were averaged over all the response DOFs to make them easier to interpret, but it is unclear if this is a valid approach. Other metrics were investigated that were easier to interpret and digest (e.g., the shock response spectrum), but these seemed to oversimplify the desired comparisons.

Conclusions and Further Work

This work demonstrated the use of CB-TPA with an advanced inverse method in a transient problem and generally replicated the findings from the previous work on random vibration environments. The auto-Tikhonov force estimation method dramatically improved the accuracy of the predicted response amplitudes, but it was found that certain inverse settings would result in apparent non-causal behavior. Unfortunately, the cause of this non-causal behavior was not identified in this work and should be studied further.

While the predicted responses from the CB-TPA process seemed reasonable, it was difficult to document the comparisons that demonstrate the prediction accuracy. It was found that detailed metrics (e.g., error spectrograms) were too overwhelming to be useful since it was difficult to track all the data in the metric. Conversely, many metrics that were more "digestible" seemed to leave out fundamental information for the accuracy evaluation. Future work should focus on developing metrics that can be used to simply quantify the response prediction accuracy in a meaningful and digestible way. High quality metrics will be critical to the advancement of time domain CB-TPA, since it is difficult to make improvements if the performance of current methods cannot be quantified.

Acknowledgments This article has been authored by an employee of National Technology & Engineering Solutions of Sandia, LLC under Contract No. DE-NA0003525 with the U.S. Department of Energy (DOE). The employee owns all right, title and interest in and to the article and is solely responsible for its contents. The United States Government retains and the publisher, by accepting the article for publication, acknowledges that the United States Government retains a non-exclusive, paid-up, irrevocable, world-wide license to publish or reproduce the published form of this article or allow others to do so, for United States Government purposes. The DOE will provide public access to these results of federally sponsored research in accordance with the DOE Public Access Plan https://www.energy.gov/downloads/doe-public-access-plan.

References

1. M. H. A. Janssens, J. W. Verheij, and D. J. Thompson, "THE USE OF AN EQUIVALENT FORCES METHOD FOR THE EXPERIMENTAL QUANTIFICATION OF STRUCTURAL SOUND TRANSMISSION IN SHIPS," Journal of Sound and Vibration, vol. 226, no. 2, pp. 305-328, 1999/09/16/ 1999, doi: https://doi.org/10.1006/jsvi.1999.2303.
2. M. H. A. Janssens, J. W. Verheij, and T. Loyau, "Experimental example of the pseudo-forces method used in characterisation of a structure-borne sound source," Applied Acoustics, vol. 63, no. 1, pp. 9-34, 2002/01/01/ 2002, doi: https://doi.org/10.1016/S0003-682X(01)00023-8.
3. A. Elliott and A. Moorhouse, "Characterisation of structure borne sound sources from measurement in-situ," The Journal of the Acoustical Society of America, vol. 123, p. 3176, 06/01 2008, doi: 10.1121/1.2933261.
4. A. T. Moorhouse, A. S. Elliott, and T. A. Evans, "In situ measurement of the blocked force of structure-borne sound sources," Journal of Sound and Vibration, vol. 325, no. 4, pp. 679-685, 2009/09/11/ 2009, doi: https://doi.org/10.1016/j.jsv.2009.04.035.
5. A. S. Elliott, A. T. Moorhouse, T. Huntley, and S. Tate, "In-situ source path contribution analysis of structure borne road noise," Journal of Sound and Vibration, vol. 332, no. 24, pp. 6276-6295, 2013/11/25/ 2013, doi: https://doi.org/10.1016/j.jsv.2013.05.031.
6. M. V. van der Seijs, D. de Klerk, and D. J. Rixen, "General framework for transfer path analysis: History, theory and classification of techniques," Mechanical Systems and Signal Processing, vol. 68-69, pp. 217-244, 2016/02/01/ 2016, doi: https://doi.org/10.1016/j.ymssp.2015.08.004.
7. S. Carter and B. Owens, "Errors using six degree-of-freedom force estimates to translate environments system-to-system," in ISMA, Leuven, BE, 2022.
8. S. Carter and B. Owens, "Using Component Based TPA to Translate Vibration Environments Between Versions of the Round Robin Structure with FRFs Derived from Analytical Models," in Proceedings of IMAC XLI, the 41st International Modal Analysis Conference, Austin, 2023.
9. S. Carter, "A look at overfitting in source estimation problems," in Proceeding of IMAC XLIII, the 43rd International Modal Analysis Conference, Orlando, 2025.
10. A. N. Thite and D. J. Thompson, "The quantification of structure-borne transmission paths by inverse methods. Part 1: Improved singular value rejection methods," Journal of Sound and Vibration, vol. 264, no. 2, pp. 411-431, 2003/07/03/ 2003, doi: https://doi.org/10.1016/S0022-460X(02)01202-6.
11. A. N. Thite and D. J. Thompson, "The quantification of structure-borne transmission paths by inverse methods. Part 2: Use of regularization techniques," Journal of Sound and Vibration, vol. 264, no. 2, pp. 433-451, 2003/07/03/ 2003, doi: https://doi.org/10.1016/S0022-460X(02)01203-8.
12. A. N. Thite and D. J. Thompson, "Selection of response measurement locations to improve inverse force determination," Applied Acoustics, vol. 67, no. 8, pp. 797-818, 2006/08/01/ 2006, doi: https://doi.org/10.1016/j.apacoust.2006.01.001.

13. H. G. Choi, A. N. Thite, and D. J. Thompson, “Comparison of methods for parameter selection in Tikhonov regularization with application to inverse force determination,” Journal of Sound and Vibration, vol. 304, no. 3, pp. 894-917, 2007/07/24/ 2007, doi: https://doi.org/10.1016/j.jsv.2007.03.040.
14. M. Aucejo and O. De Smet, “Bayesian source identification using local priors,” Mechanical Systems and Signal Processing, vol. 66-67, pp. 120-136, 2016/01/01/ 2016, doi: https://doi.org/10.1016/j.ymssp.2015.05.004.
15. M. Aucejo and O. De Smet, “On a full Bayesian inference for force reconstruction problems,” Mechanical Systems and Signal Processing, vol. 104, pp. 36-59, 2018/05/01/ 2018, doi: https://doi.org/10.1016/j.ymssp.2017.10.023.
16. M. Aucejo and O. De Smet, “An optimal Bayesian regularization for force reconstruction problems,” Mechanical Systems and Signal Processing, vol. 126, pp. 98-115, 2019/07/01/ 2019, doi: https://doi.org/10.1016/j.ymssp.2019.02.021.
17. S. Carter, “Thoughts on Using Sparse Inverse Solutions in Transfer Path Analysis,” in Proceedings of IMAC XLII, the 42nd International Modal Analysis Conference, Orlando, 2024.
18. P. E. Bofinger, J. Boelens, S. W. B. Klaassen, and D. de Klerk, “X-DoF: Automatic Degree-of-Freedom Subset Selection for Inverse Blocked Force Characterization,” Journal of Vibration and Acoustics, vol. 147, no. 1, 2024, doi: 10.1115/1.4067081.
19. D. Roettgen and A. Linderholt, “Substructuring excercises on combinations of steel and aluminum components of the benchmark structure of the technical division on dynamic substructures,” in The 40th International Modal Analysis Conference, Orlando, 2022.
20. D. Roettgen, G. Lopp, A. Jaramillo, and B. Moldenhauer, “Experimental Substructuring of the Dynamic Substructures Round-Robin Testbed,” 2022, pp. 119-123.
21. D. Rohe and R. Schultz, “Rattlesnake: An open-source multi-axis and combined evironments vibration controller,” in Proceedings of IMAC-XL, the 40th International Modal Analysis Conference, Orlando, 2022.
22. D. Rohe, “SDynPy: A Structural Dynamics Python Library,” in Proceedings of IMAC XLI, the 41st International Modal Analysis Conference, Austin, 2023.
23. S. Carter and D. Rohe, “Inverse Source Estimation Tools in SDynPy, an Open-Source Python Package,” Cham, 2025: Springer Nature Switzerland, in Dynamic Substructures, Vol. 4, pp. 111-123.
24. W. H. Press, S. A. Teukolsky, W. T. Vetterling, and B. P. Flannery, Numerical Recipes in FORTRAN 77: Volume 1, Volume 1 of Fortran Numerical Recipes: The Art of Scientific Computing. Cambridge: Cambridge University Press, 1992.
25. R. J. Thornhill and C. C. Smith, “Time Aliasing: A Digital Data Processing Phenomenon,” Journal of Dynamic Systems, Measurement, and Control, vol. 105, no. 4, pp. 232-237, 1983, doi: 10.1115/1.3140664.
26. R. Schultz, “A Demonstration of Force Estimation and Regularization Methods for Multi-Shaker Testing,” 2020, pp. 229-243.
27. L. N. Trefethen and D. Bau, III, Numerical Linear Algebra. Philadelphia: Society for Industrial and Applied Mathematics, 1997.
28. K. Coletti, S. Carter, and R. Schultz, “FRF Error Mitigation Methods for Time Waveform Replication,” in the 43rd International Modal Analysis Conference, Orlando, FL, 2025.
29. M. Zvonkin, “Methods for checking and enforcing physical quality of linear electrical network models,” Master of Science in Electrical Engineering, Electrical Engineering, MISSOURI UNIVERSITY OF SCIENCE AND TECHNOLOGY, 2015.
30. S. Carter. “ForceFinder.” https://github.com/sandialabs/forcefinder (accessed 2025).
31. MIL-STD-810H: Environmental Engineering Considerations and Laboratory Tests. US Military, 2019.